



Interfacial Solid–Liquid Reaction of Ni/In/Ni Structure During Isothermal Reflow Process

Yen-Jui Cheng¹ · Cheng-Hsin Lu¹ · Fan-Yi Ouyang¹

Received: 2 June 2021 / Accepted: 20 September 2021 / Published online: 23 October 2021
© The Minerals, Metals & Materials Society 2021

Abstract

In electronic packaging technology, intermetallic compounds (IMCs) formed during a reflow process significantly affect the mechanical properties of the devices. In this study, In solder and Ni under-bump metallization (UBM) were chosen to investigate the solid–liquid interfacial reaction under an isothermal reflow process. Two types of IMCs, uniform and scallop-type, were formed in turn after being reflowed at three different temperatures, 220°C, 250°C, and 280°C. Elemental analysis has revealed that the compositions of both types of IMCs are nearly the same and were eventually identified as Ni₃In₇. By the growth rate of IMC formation, the mechanism of the growing process was proposed to be a diffusion-controlled process. The activation energy (*Q*) of the IMC formation was calculated to be 83.8 $\frac{\text{kJ}}{\text{mol}}$.

Keywords Intermetallic compound (IMC) · Ni under-bump metallization (UBM) · In-based solder · solid–liquid interdiffusion (SLID) bonding

Introduction

Three-dimensional integrated circuits (3D ICs) have recently been widely discussed in the chip packaging industry. Because there is a high demand for increased density of transistors that can fit on a single chip, the die size of 3D ICs has decreased, enabling better performance in electronic devices. When chips are packaged together, a reflow process is an indispensable step to ensure that the chips can be bonded together. During a reflow process, intermetallic compounds (IMCs) are formed to connect solder and under-bump metallization (UBM) material. IMCs are defined as solid phases containing two or more metallic or non-metallic elements, with crystal structures distinct from other compounds.¹ The properties and thickness of IMCs significantly affect the electrical, thermal, and mechanical properties of the devices; however, IMCs can also have negative effects on the devices, such as introducing brittleness that affects the bonding reliability if the bonding condition was not well controlled.² These issues give rise to phenomena such as thermomigration and electromigration.^{3,4} Thermomigration

occurs when a thermal gradient is formed, which can have a huge effect on the diffusion between the elements. A thermal gradient can lead to abnormal growth of IMCs at the cold end and significant dissolution of UBM at the hot side.^{5,6} Electromigration is also an important mechanism in integrated circuits, as a process of ionic movement which causes the interconnects to wear out and at the same time can make the ICs more unreliable.^{7–9} Thus, understanding the growth behavior of IMCs during a reflow process is critical.

Due to environmental and health issues, most industries have stopped using lead-based soldering materials.^{10,11} Thus alternatives to lead are now the primary material for soldering technology. Indium has previously been used in the semiconductor industry in various ways, for example, as seals under a high-vacuum,¹² transparent conductive coatings of indium tin oxide (ITO), and solders due to its low melting point (approximately 156 °C).¹³ When used as solder, indium provides some advantageous properties. For example, the addition of indium can improve the wettability of lead-free solder.¹⁴ Moreover, it increases the melting range and lowers the liquidus and solidus temperatures.¹⁵ In addition, nickel commonly serves as a UBM material and a diffusion barrier in solder joints in packaging technology due to its relatively slow reaction rate with solders.¹⁶ There have been many studies exploring the intermetallic compound properties in different lead-free solders, such as SnAgCu,

✉ Fan-Yi Ouyang
fyouyang@ess.nthu.edu.tw

¹ Department of Engineering and System Science, National Tsing Hua University, Hsinchu 30013, Taiwan

SnAg, and SnCu solders.^{17–19} There are also studies discussing the effect of the addition of In or Cu/Ni in the Sn-rich solder.^{20,21} Despite all the promising properties of indium, however, there have only been a few studies investigating the interfacial reaction between nickel and indium.²²

In this study, the solid–liquid interfacial reaction of the Ni/In/Ni sandwich structure was investigated. The microstructural evolution of IMCs formed between In-based solder and Ni substrate was examined at different reflow temperatures. In addition, the characteristics of the morphologies and the growth kinetics of IMCs were explored. Elemental analysis was employed to identify the phase of IMCs, and the activation energy was also calculated.

Experimental Procedures

The symmetrical sandwich structure Ni/In/Ni specimens were used to investigate the solid–liquid interfacial reaction during an isothermal reflow process. We first prepared 12-inch wafers which were sputtered with Cu and Ti as an adhesive layer. Ni was then electroplated on the adhesive

layer (ca. 5 μm). The wafers were cut into 1 cm \times 1 cm chips. In foil with purity of 99.99% and thickness of 50 μm (Nilaco Corporation) was clamped between two Si chips by a special holder with no soldering flux applied (Fig. 1a). The reason for choosing relatively thin Ni layers to combine with a thick In layer is to mimic the spatial geometry of the actual UBM pad/solder bump size in real-world applications. Finally, the specimens of the Ni/In/Ni sandwich structure were obtained, and the schematic representation of the chip sample is shown in Fig. 1b.

The specimens were placed on a pre-heated hot plate to reflow under isothermal conditions. Three different bonding temperatures, namely 220°C, 250°C, and 280°C, were chosen with different reflow times. For samples bonding at 220°C and 250°C, reflow times ranging from 15 min, 30 min, 60 min, 90 min, 120 min, 150 min, and 180 min were studied. For samples bonding at 280°C, reflow times of 15 min, 30 min, 45 min, 60 min, and 90 min were studied.

After being reflowed, the specimens were first removed from the hot plate and left to cool to room temperature. Each specimen was ground by SiC papers with grit sizes from 800 to 4000 in sequence and then polished by Al_2O_3 suspensions

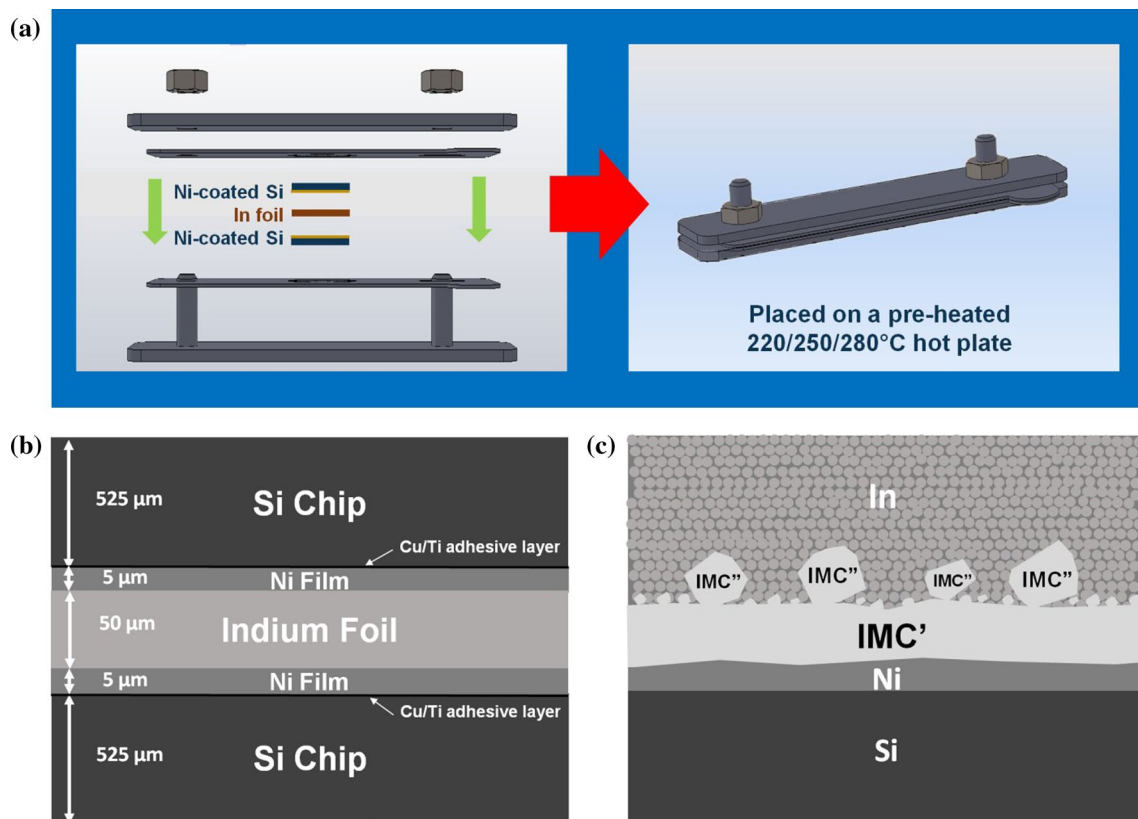


Fig. 1 Schematic representation of (a) the experimental setup of the special clamp holder designed for the experiment, (b) the Ni/In/Ni sandwich structure between two silicon chips that undergoes the reflow process (not to scale), and (c) two types of IMC structures

grown in the Ni/In/Ni sandwich structure after being reflowed for a certain length of time. IMC' represents the uniform type of IMCs, while IMC'' represents scallop-type IMCs.

with particle sizes from 0.3 μm to 0.05 μm in sequence. Finally, a JEOL JSM-6500F field emission scanning electron microscope (FE-SEM, JEOL Ltd. Tokyo, Japan) equipped with a low-angle backscatter electron (LBE) detector was used to observe the microstructure, phase contrast, and morphological evolution of the cross-section of the specimens. Energy-dispersive X-ray spectroscopy (EDX) was utilized to analyze the elemental concentration of the profile. After the SEM images were obtained, image processing software (ImageJ) was employed to determine the thickness of the IMC growth on each side. By integrating the area of the IMC layer within the image (either the top side or the bottom side) using ImageJ and then dividing it by the length of the IMC (the width of the image), the average thickness of the IMC was obtained. Since the top and the bottom sides were very close to each other, they were treated as reflowed under the same temperature conditions, and therefore the final mean IMC thicknesses were calculated by averaging the obtained IMC thickness at the top and bottom sides.

Results and Discussion

Generally speaking, the growth rate of the IMC layer increases as the temperature increases because the diffusion rates are faster at a higher temperature.²² A schematic representation (Fig. 1c) and SEM images of the microstructures of the Ni/In/Ni sandwich structure after being reflowed under 220°C (Fig. 2), 250°C (Fig. 4), and 280°C (Fig. 5) for different times are displayed. Figure 2 represents SEM images of the specimens which were subjected to a reflow temperature of 220°C for different times, i.e., 15 min, 30 min, 60 min, 90 min, 120 min, 150 min, and 180 min. It can be observed that the IMCs become symmetrically thicker as time increases. The growth directions of the interfacial IMCs on either side are both toward the middle. When the reflow process is about 30 to 60 min, a second layer of IMC starts to form. It can be seen that the first layer of IMC is more uniform (as the IMC' demonstrated in Fig. 1c) while the second layer is scallop-shaped (as the IMC'' demonstrated in Fig. 1c). There are also small holes between the first layer and the second layer. As the reflow time increases, the scallop-shaped IMCs in the second layer increase in size, while the uniform layer of interfacial IMC becomes thicker.

To further investigate the composition of both types of IMCs on either side, EDX elemental analysis was used to analyze these two types of IMC layers, and some examples of the results can be seen in Fig. 3. In 15 min, these very thin layers of IMCs contain about 45 at% In and can thus be inferred as the NiIn phase of the IMC. After 30 min, the percentage of In in both types of IMCs increases to about 70 at%, which suggests the formation of the Ni_3In_7 phase of the IMC. This indicates that In atoms have diffused into the

IMC layer constantly in both types of layers. The literature has also shown that Ni-In couples tend to form IMCs with an atomic ratio of Ni:In close to 30:70 at a temperature ranging between 250° and 300°C.²² From 60 min to 180 min, the proportion of In in both types of IMCs reaches about 80 at% and is identified as the Ni_3In_7 phase containing supersaturated indium. When the internal stress accumulated overcomes the energy barrier necessary for nucleation of the new phase, such a nucleus allows part of the excess indium in the solid solution to diffuse to the new phase seed to decrease the stresses in the original solid solutions and energetically favoring new IMC formation.²³ Similar results were found in the Cu-In couples, where an indium-oversaturated $\text{Cu}_{11}\text{In}_9$ phase was found in the early stage of the reaction.²⁴

Figure 4 shows SEM images of the specimens which were subjected to a reflow temperature of 250°C at different times, namely 15 min, 30 min, 60 min, 90 min, 120 min, 150 min, and 180 min. In these figures, we can observe that at 15 min, two types of layers have already formed. There are also still some small holes between the two types of layers. These small holes are due to the formation of individual small IMC grains. The small grains fuse together forming larger grains (i.e., scallop-type IMCs) due to Ostwald ripening, while the holes start to shrink and even disappear over time.²⁵ EDX analysis reveals that nearly all layers formed on both sides of specimens contain a percentage of In at around 80 at% and Ni at around 20 at%. By referring to the phase diagram of Ni and In, we infer that the most likely IMC formed on both sides in the phase diagram was Ni_3In_7 with supersaturated indium. Under temperature of 250 °C, we can observe that the elemental composition of the IMC can reach the same Ni/In ratio faster than in the 220 °C cases. This is probably because the higher temperature can generate a higher driving force, which decreases the time required for the IMCs to be stabilized.

Figure 5 presents SEM images of the specimens which were subjected to a reflow temperature of 280°C at different times of 15 min, 30 min, 40 min, 60 min, and 90 min. An observable IMC layer has formed symmetrically within 15 min. Scallop-shaped IMCs and uniform IMCs can also be seen after only 15 min. We choose the smaller intervals of reflow time because of the higher temperature, which is expected to provide a higher driving force that allows the IMCs to form more rapidly than those reflowed at 220 °C and 250 °C. As previous specimens showed, the IMC layers of these samples subjected to 280 °C eventually grow quite thick and symmetrical as time increases. In the last sample of reflow time after 90 min, it can even be noted that a small part of scallop-type IMCs has detached from the lower side of the interface. We deduced that the phenomenon of IMC spalling was either due to the poor adhesion between the two interfaces or for the system to reduce their interfacial free energy.^{26,27} EDX was also used to analyze the composition

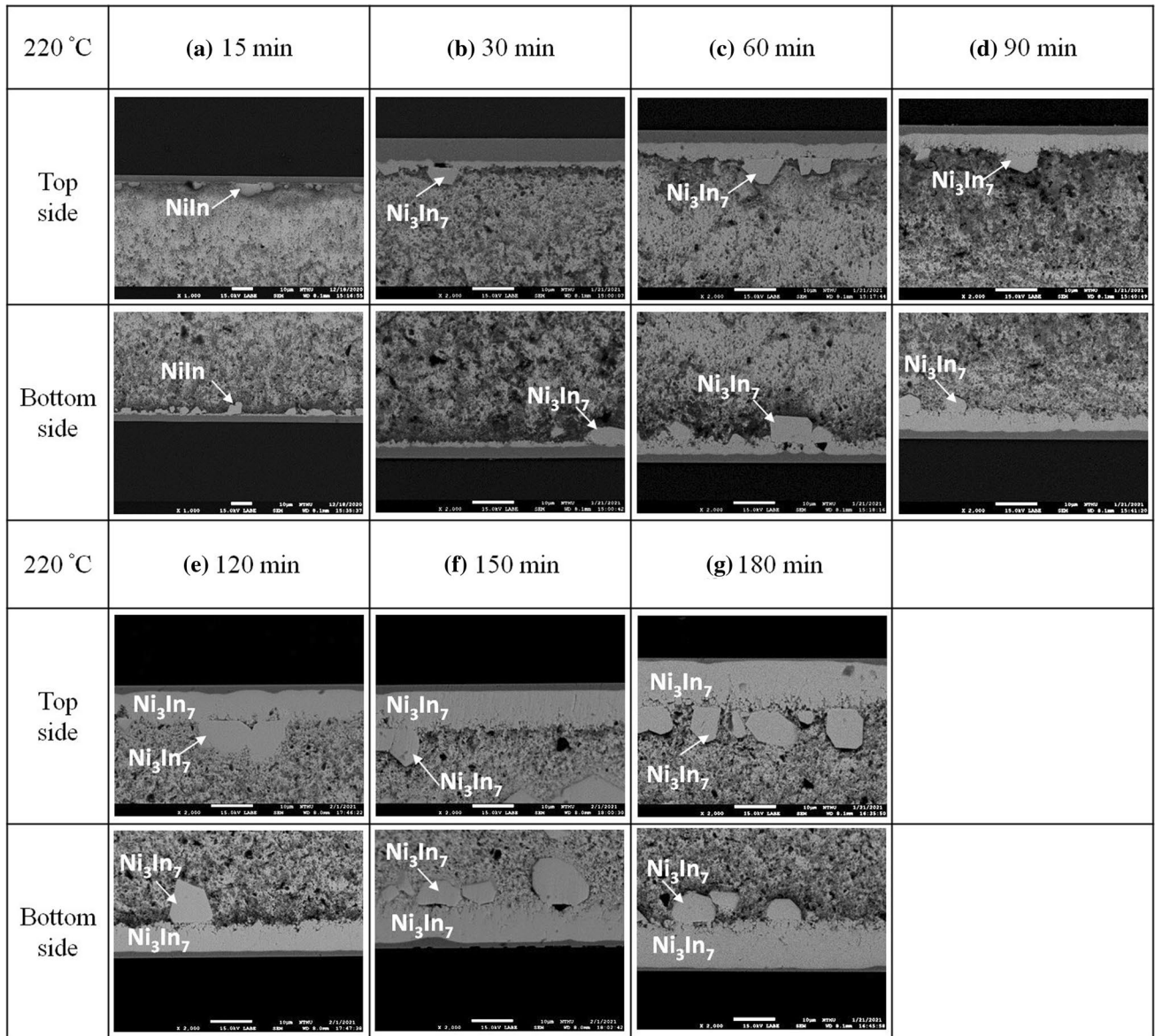


Fig. 2 SEM images of the microstructure of non-in situ Ni/In/Ni sandwich structure samples reflowed under a 220°C isothermal bonding process for (a) 15 min, (b) 30 min, (c) 60 min, (d) 90 min, (e) 120 min, (f) 150 min, and (g) 180 min. The scale bars represent 10 μm .

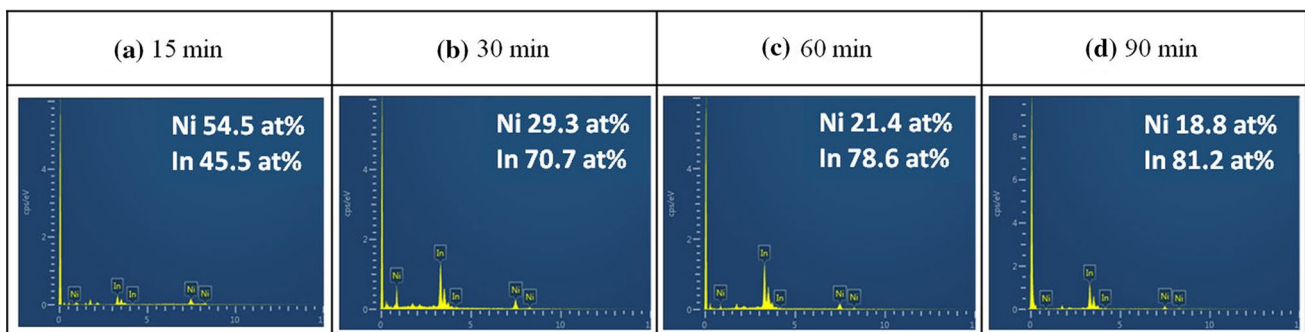


Fig. 3 Some examples of the EDX spectra and elemental analysis results of the IMC layers for chips reflowed at 220°C after 15 to 90 min.

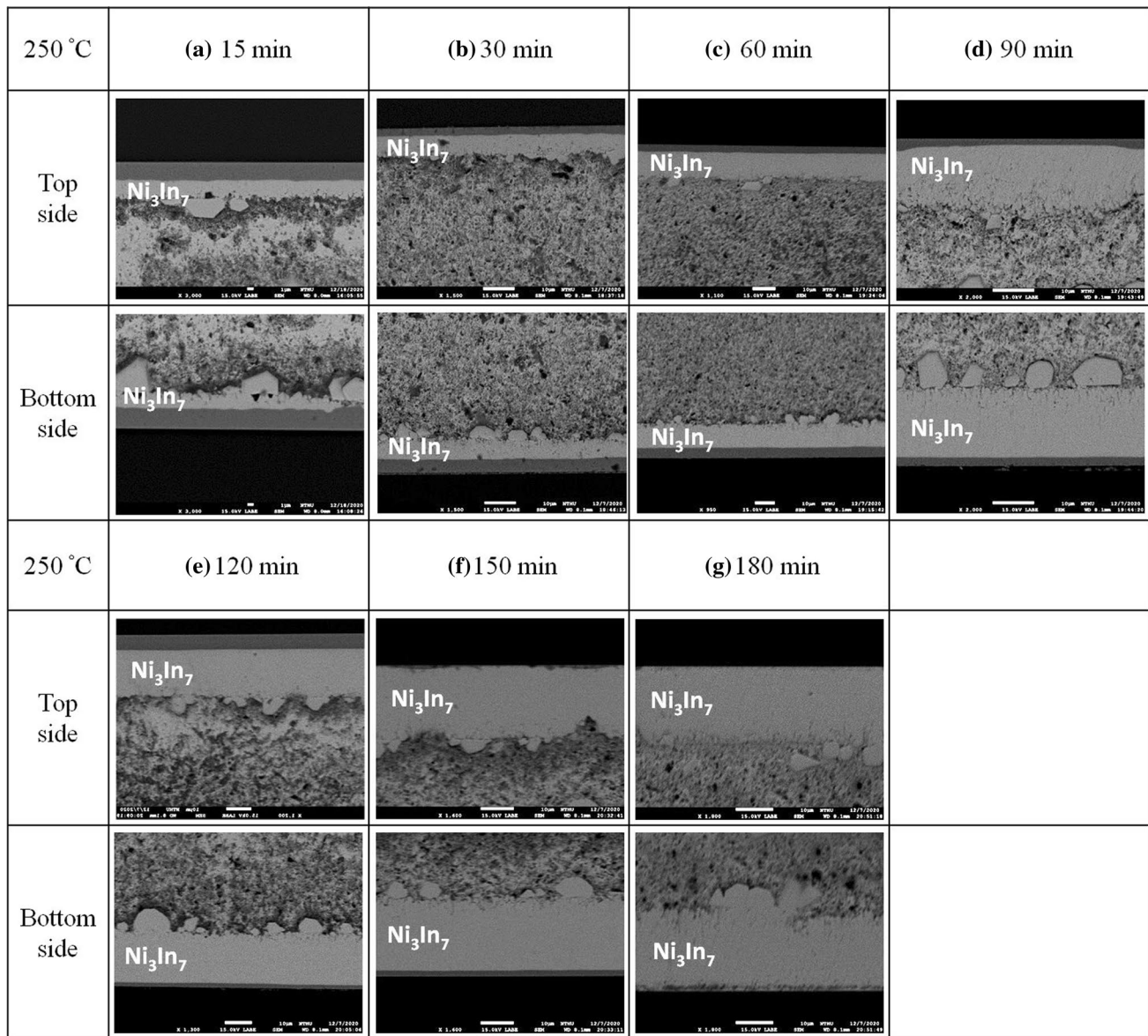


Fig. 4 SEM images of the microstructure of non-in situ Ni/In/Ni sandwich structure samples reflowed under a 250 °C isothermal bonding process for (a) 15 min, (b) 30 min, (c) 60 min, (d) 90 min, (e) 120 min, (f) 150 min, and (g) 180 min. The scale bars represent 10 μm .

of these IMC layers. A percentage of In at around 80 at.% and Ni at around 20 at.% is also detected in these specimens. Similar to the specimens reflowed at 250°C, this IMC was categorized as Ni_3In_7 containing supersaturated indium.

When reflowed at 220°C, 250°C, and 280°C, the composition of the IMCs formed on both sides of all specimens eventually reached the Ni_3In_7 phase. We inferred that higher temperatures cause the IMCs to be more indium-saturated. Since there is no temperature gradient across the specimen during the reflow process, the chemical potential gradient is the main driving force during isothermal annealing. In the evolution of the IMC morphology, it can be found that, on both sides, as long as the sample has been

reflowed for enough time, two types of IMCs are formed: a uniform type and a scallop type. This indicates that large scallop-type IMCs need a certain amount of time to form, and a higher reflow temperature can decrease the formation time required. If the temperature is high enough, two types of interfacial IMCs can form within a short period of time, as shown in Fig. 5. Both types of IMCs on both sides contain similar composition of Ni and In. Although in the early stage the interfacial IMC may contain an unstable composition (such as the NiIn phase in the 15-min case of the sample under the 220°C reflow process), these IMCs will eventually maintain a fixed composition and can be categorized as Ni_3In_7 phase in the phase diagram of In

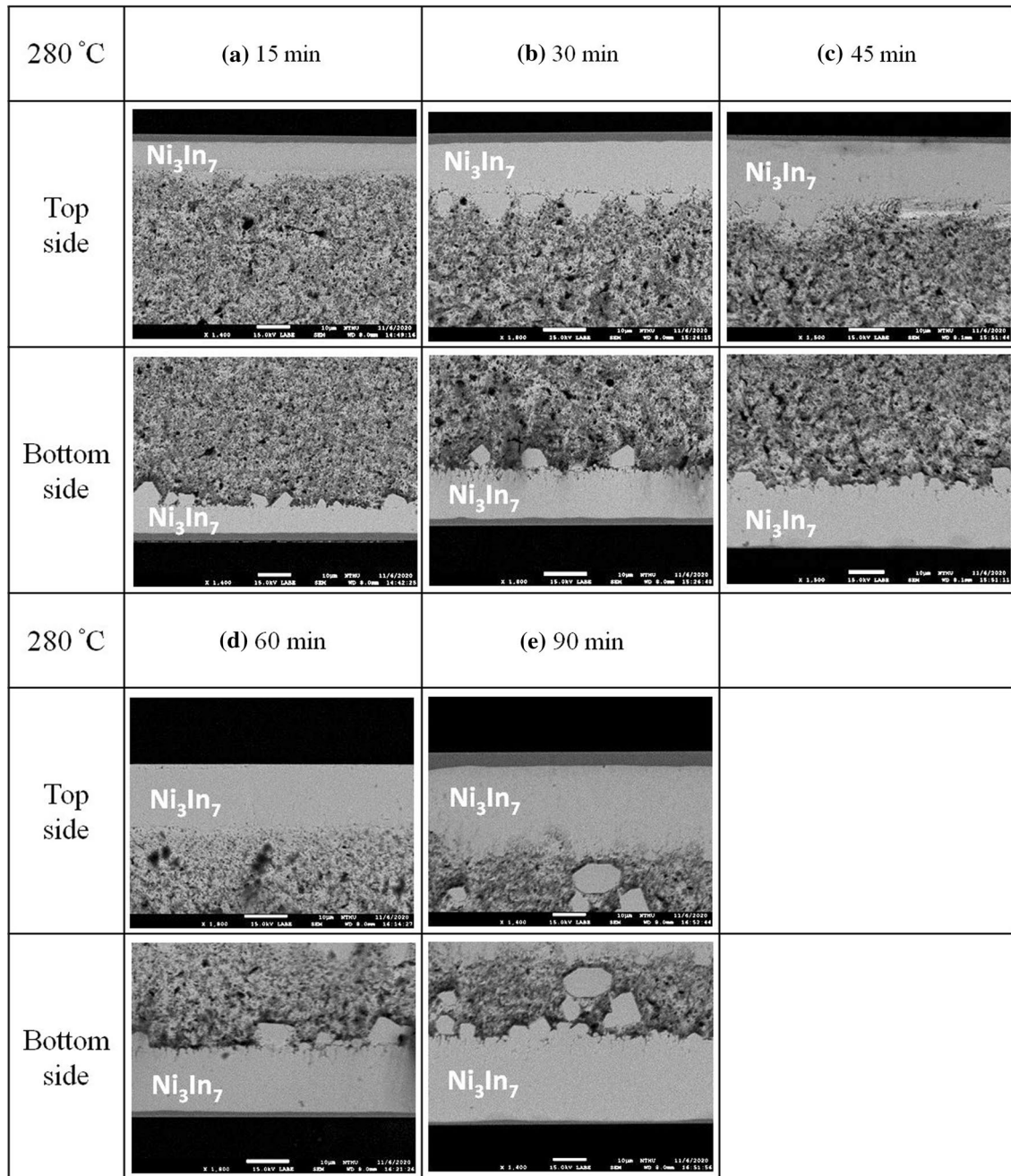


Fig. 5 SEM images of the microstructure of non-in situ Ni/In/Ni sandwich structure samples reflowed under a 280°C isothermal bonding process for (a) 15 min, (b) 30 min, (c) 45 min, (d) 60 min, and (e) 90 min. The scale bars represent 10 μm .

and Ni. As for the small holes between the two types of IMCs on both sides, their existence might be attributed to the difference in the surface energy between the two types of IMCs. With increasing time, the individual small scallop-type IMC grains fuse together, forming larger scallop-type IMC grains, and the difference in the surface energy between the uniform IMCs and scallop-type IMCs decreases; therefore, the interface between the two types of IMCs becomes more uniform.

Figure 6a and Table I show the mean thickness of the IMC during the isothermal reflow process at 220°C, 250°C, and 280°C for different times. The mean thickness of the IMC layer at the reaction interface is determined by dividing the total area of the reaction layer by the horizontal length of the selected area, then averaging the results obtained from the top side and the bottom side. The average thicknesses obtained in this way can prevent selection bias introduced by choosing different individual points during measurements.

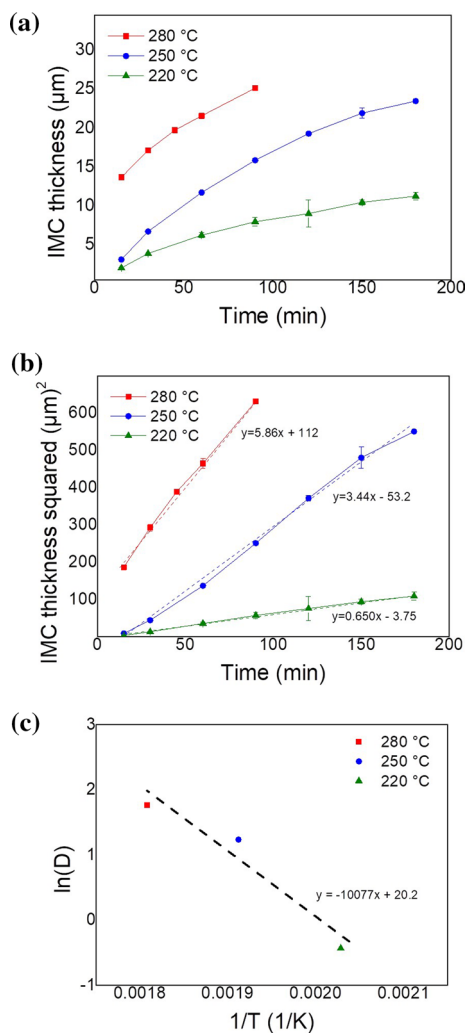


Fig. 6 (a) Mean measured thicknesses and (b) thickness squared of the Ni–In IMCs during an isothermal reflow process at 220°C, 250°C, and 280°C as a function of different reflow times. (c) Natural log of the three different diffusion constants at 220°C, 250°C, and 280°C as a function of the inverse temperature. Note that the thickness deviations between the top and bottom sides are very small, so that most of the error bars in (a) and (b) are covered by the point symbols and cannot be seen. The mean thicknesses and standard deviations in (a) are summarized in Table I.

It is observed that the thicknesses of the interfacial IMC layers on both sides of specimens follow the parabolic law, where the thickness of IMCs is proportional to the square root of the time (Fig. 6b). Thus, the atomic diffusion of Ni and In was the main controlling mechanism of the growth of the IMC.

Fig. 6b shows the graph of IMC thickness squared versus time. It can be seen that the thickness squared is proportional to time. Therefore, it can be inferred that the whole isothermal annealing process was a diffusion-controlled process.²⁸ Thus, the relationship between thickness and time can be expressed as the equation

$$X = X_0 + \sqrt{Dt}, \tag{1}$$

where X represents the IMC thickness in micrometers, X_0 represents the initial IMC thickness, D is the diffusion constant, and t is the reflow time in minutes. The values of IMC thickness can be obtained using ImageJ software as mentioned previously. By inserting linear regression lines in the diagram, the slope of the trend line for the three different temperatures, 220°C, 250°C, and 280°C, can be obtained through the linear regression equation

$$y = mx + b, \tag{2}$$

yielding values of $0.650 \mu\text{m}/\text{min}^2$, $3.44 \mu\text{m}/\text{min}^2$, and $5.86 \mu\text{m}/\text{min}^2$, respectively, which also represent the diffusion constant of Ni atoms in In under different temperatures. The y-intercepts of the equations for 220°C and 250°C were both negative, which suggests that from the extrapolation of the existing data, the IMCs under these two temperatures need an incubation time to form (i.e., a positive x (time) is required to obtain a y (thickness) ≥ 0). However, at 280°C, the y-intercept of the equation was positive, and therefore we can reasonably infer that the temperature was high enough that the incubation time for IMC formation can be ignored. The literature has also shown that the incubation time for the formation of Ni–In IMC decreases with increasing temperature [22].

Since the IMC formation was a thermally activated process, the Arrhenius equation is introduced to further investigate the three different diffusion constants at three different temperatures. The equation can be expressed as

Table I Summary of mean measured thicknesses of the Ni–In IMCs during an isothermal reflow process at 220°C, 250°C, and 280°C as a function of different reflow times

220°C	15 min	30 min	60 min	90 min	120 min	150 min	180 min
Thickness (μm)	2.03 ± 0.09	3.87 ± 0.01	6.23 ± 0.30	7.96 ± 0.54	9.01 ± 1.75	10.46 ± 0.33	11.25 ± 0.47
250°C	15 min	30 min	60 min	90 min	120 min	150 min	180 min
Thickness (μm)	3.10 ± 0.18	6.70 ± 0.06	11.72 ± 0.09	15.86 ± 0.09	19.28 ± 0.20	21.92 ± 0.65	23.47 ± 0.06
280°C	15 min	30 min	45 min	60 min	90 min		
Thickness (μm)	13.67 ± 0.20	17.12 ± 0.26	19.73 ± 0.09	21.57 ± 0.29	25.13 ± 0.11		

Table II Diffusion constant (D) and activation energy (Q) during Ni-In interfacial reaction.

Temperature	D ($\frac{\mu\text{m}^2}{\text{min}}$)	Q ($\frac{\text{kJ}}{\text{mol}}$)
220°C	0.650	83.8
250°C	3.44	83.8
280°C	5.86	83.8

$$D = D_0 \exp\left(\frac{-Q}{RT}\right), \quad (3)$$

where D is the diffusion constant, D_0 is a pre-exponential frequency factor, Q is the activation energy, R is the gas constant ($8.3145 \frac{\text{J}}{\text{mol K}}$), and T is the temperature (K). By taking the natural log of the three different diffusion constants, which were -0.431 , 1.24 , and 1.77 , respectively, we can draw a diagram as a function of the inverse temperature values $\frac{1}{T}$, which were 0.00203 , 0.00191 , and 0.00181 , respectively. As shown in Fig. 6c, the slope of the trend line represents $-\frac{Q}{R}$ and is calculated as $-10,077$. Thus, by multiplying by the gas constant, $8.3145 \frac{\text{J}}{\text{mol K}}$, we can obtain the activation energy of Ni-In IMC formation to be $83.8 \frac{\text{kJ}}{\text{mol}}$ (Table II), which is in the same order as the activation energy obtained in the literature [22].

Conclusions

In summary, this study investigated interfacial reaction and microstructure evolution of Ni-In IMCs during the isothermal reflow process using a Ni/In/Ni sandwich structure as a model. Their interfacial reaction was tested under three different reflow processes, each of which was at a fixed temperature of 220°C, 250°C, or 280°C. After carefully examining the images of the interfacial microstructure, two types of IMC morphologies were identified, one of which was a uniform type and the other which was a scallop-shaped type. Both types of interfacial IMCs eventually retained the specific form of IMC as Ni_3In_7 . By noting the relationship between the thickness of the interfacial IMC and reflow time, we can conclude that there is a diffusion-controlled mechanism, and the activation energy of the interfacial Ni_3In_7 IMC is calculated to be $83.8 \frac{\text{kJ}}{\text{mol}}$.

Acknowledgments The authors are grateful for the funding support from the Ministry of Science and Technology of Taiwan, R.O.C., under contract nos. 108-2221-E-007-055-MY3 and 110-2811-M-007-507. The authors would also like to thank the Instrumentation Center at National Tsing Hua University (NTHU) for their JEOL JSM-6500F Field Emission Scanning Electron Microscope analysis.

Conflict of interest The authors declare that they have no conflict of interest.

References

1. P. Haasen, G.E.R. Schulze: Metallphysik. Akademie-Verlag, Berlin 1967. 458 Seiten, 30 Tabellen, 227 Abbildungen. Preis: DM 48,—Berichte der Bunsengesellschaft für physikalische Chemie 72(2), 359 (1968).
2. T. An, and F. Qin, *Effects of the Intermetallic Compound Microstructure on the Tensile Behavior of Sn3.0Ag0.5Cu/Cu Solder Joint Under Various Strain Rates Microelectron. Reliab.* 54, 932 (2014).
3. Y.-F. Lin, Y.-C. Hao, and F.-Y. Ouyang, *Improvement of Thermomigration Resistance in Lead-Free Sn3.5Ag Alloys by Ag Interlayer J. Alloys Compd.* 847, 156429 (2020).
4. F.-Y. Ouyang, G.-L. Hong, Y.-R. Hsu, S.-Y. Mao, and W.-J. Liu, *Thermomigration in Co/SnAg/Co and Cu/SnAg/Co Sandwich Structure Microelectron. Reliab.* 97, 16 (2019).
5. C. Chen, H.-Y. Hsiao, Y.-W. Chang, F. Ouyang, and K.N. Tu, *Thermomigration in Solder Joints Mater. Sci. Eng., R* 73, 85 (2012).
6. X. Gu, and Y.C. Chan, *Thermomigration and Electromigration in Sn58Bi Solder Joints J. Appl. Phys.* 105, 093537 (2009).
7. Y.-H. Liao, C.-H. Chen, C.-L. Liang, K.-L. Lin, and A.T. Wu, *A Comprehensive Study of Electromigration in Pure Sn: Effects on Crystallinity, Microstructure, and Electrical Property Acta Mater.* 200, 200 (2020).
8. Z. Zhang, X. Hu, X. Jiang, and Y. Li, *Influences of Mono-Ni(P) and Dual-Cu/Ni(P) Plating on the Interfacial Microstructure Evolution of Solder Joints Metall. Mater. Trans. A* 50, 480 (2019).
9. P. Zhang, S. Xue, and J. Wang, *New Challenges of Miniaturization of Electronic Devices: Electromigration and Thermomigration in Lead-Free Solder Joints Mater. Des.* 192, 108726 (2020).
10. M. AbdelAziz, D.E. Xu, G. Wang, and M. Mayer, *Electromigration in Solder Joints: A Cross-Sectioned Model System for Real-time Observation Microelectron. Reliab.* 119, 114068 (2021).
11. A. Kunwar, Y.A. Coutinho, J. Hektor, H. Ma, and N. Moelans, *Integration of Machine Learning with Phase Field Method to Model the Electromigration Induced Cu6Sn5 IMC Growth at Anode side Cu/Sn Interface J. Mater. Sci. Technol.* 59, 203 (2020).
12. H. Saeki, J. Ikeda, and H. Ishimaru, *Optical Window Sealed with Indium for Ultrahigh Vacuum Vac.* 39, 563 (1989).
13. T. Wang, S. Li, B. He, X. Zhu, Y. Luo, Q. Liu, T. Li, S. Lu, C. Ye, A.M. Asiri, and X. Sun, *Commercial Indium-tin Oxide Glass: A Catalyst Electrode for Efficient N2 Reduction at Ambient Conditions Chin. J. Catal.* 42, 1024 (2021).
14. L.F. Li, Y.K. Cheng, G.L. Xu, E.Z. Wang, Z.H. Zhang, and H. Wang, *Effects of Indium Addition on Properties and Wettability of Sn-0.7Cu-0.2Ni Lead-Free Solders Mater. Des.* 64, 15 (2014).
15. K. Kanlayasiri, M. Mongkolwongrojn, and T. Ariga, *Influence of Indium Addition on Characteristics of Sn-0.3Ag-0.7Cu Solder Alloy J. Alloys Compd.* 485, 225 (2009).
16. Y.-C. Tseng, H. Lee, S.-C. Tsai, Y.-W. Yen, and C.-M. Chen, *Suppression Effect of Ni Grain Size on the Ni3Sn4 Growth at the Sn/Ni Interface Mater. Charact.* 128, 232 (2017).
17. Y.-A. Shen, F.-Y. Ouyang, and C. Chen, *Effect of Sn Grain Orientation on Growth of Cu-Sn Intermetallic Compounds During Thermomigration in Cu-Sn23Ag-Ni Microbumps Mater. Lett.* 236, 190 (2019).

18. Y.-S. Yang, C.-J. Yang, and F.-Y. Ouyang, *Interfacial Reaction of Ni₃Sn₄ Intermetallic Compound in Ni/SnAg Solder/Ni System Under Thermomigration* *J. Alloys Compd.* 674, 331 (2016).
19. F.-Y. Ouyang, and Y.-P. Su, *Growth Kinetic of Ag₃Sn Intermetallic Compound in Micro-scale Pb-Free Solder Alloys Under a Temperature Gradient* *J. Alloys Compd.* 655, 155 (2016).
20. A. Sharif, and Y.C. Chan, *Effect of Indium Addition in Sn-rich Solder on the Dissolution of Cu metallization* *J. Alloys Compd.* 390, 67 (2005).
21. K.D. Min, C.J. Lee, B.U. Hwang, J.H. Kim, J.H. Jang, and S.B. Jung, *Hybrid Transient Liquid Phase Sintering Bonding of Sn-3.0Ag-0.5Cu Solder with Added Cu and Ni for Cu-Ni Bonding* *Appl. Surf. Sci.* 551, 149396 (2021).
22. Y.H. Tseng, M.S. Yeh, and T.H. Chuang, *Interfacial Reactions Between Liquid Indium and Nickel Substrate* *J. Electron. Mater.* 28, 105 (1999).
23. D. Liang, B. Unveroglu, and G. Zangari, *Electrodeposition of Cu-In Alloys as Precursors of Chalcopyrite Absorber Layers* *J. Electrochem. Soc.* 161, D613 (2014).
24. S.-W. Chen, T.-C. Yang, J.-M. Lin, and T.-Y. Huang, *Interfacial Reactions in the Co/In/Cu and Ni/In/Cu Samples* *J. Taiwan Inst. Chem. Eng.* 97, 356 (2019).
25. S. Norainiza, S.I. Najib, M.A.A. Mohd Salleh, *Low and High Temperature Isothermal Aging Effect on Morphology and Diffusion Kinetics of Intermetallic Compound (IMC) for Sn-Cu-Si₃N₄ Composite Solder*. *Key. Engz. Mater.* 666, 594-595 (2014).
26. J.-W. Jang, L.N. Ramanathan, J.-K. Lin, and D.R. Frear, *Spalling of Cu₃Sn Intermetallics in High-lead 95Pb5Sn Solder Bumps on Cu Under Bump Metallization During Solid-State Annealing* *J. Appl. Phys.* 95, 8286 (2004).
27. H. Chen, Y.-L. Tsai, Y.-T. Chang, and A.T. Wu, *Effect of Massive Spalling on Mechanical Strength of Solder Joints in Pb-Free Solder Reflowed on Co-Based Surface Finishes* *J. Alloys Compd.* 671, 100 (2016).
28. A.M. Huntz, *Parabolic Laws During High Temperature Oxidation: Relations with the Grain Size and Thickness of the Oxide* *J. Mater. Sci. Lett.* 18, 1981 (1999).

Publisher's Note Springer Nature remains neutral with regard to jurisdictional claims in published maps and institutional affiliations.